PHYSICAL SCIENCES

Microbubble-induced erosion releases micro- and nanoplastics into water

Dunzhu Li[1,2,3]*, Varvara Bolikava[2,4], Yunhong Shi[3], Songheng Jin[1], Richard Unitt[5], Emmet D. Sheerin[2,6], Peiying Kang[2,3], Liwen Xiao[3,7]*, Xiaocheng Pan[1], Christopher Hill[2,6], Manuel Ruether[6], Linfei Zhao[1], Qidong Yin[8], Bo Zhao[9], Qiliang Zhu[1], Hua Qin[1], Ming Cheng[2,3], John E. Sader[10], Jing Jing Wang[2,11]*, John J. Boland[2,6]*

Micro- and nanoplastics (MNPs) are pervasive micropollutants in aquatic environments and along shorelines. Their release is predominantly attributed to mechanical abrasion or ultraviolet exposure, both requiring substantial external energy inputs. The role of aquatic factors (e.g., air bubbles) in the generation of MNPs is poorly understood. Here we show microbubbles that spontaneously form on seven typical plastics across a wide temperature range (25° to 95°C) and in various water types (deionized, tap, river, and marine water) can erode plastic surfaces and drive MNP release. Nucleation, expansion, and movement of microbubbles generate shear stresses capable of dislodging polymer protrusions at surface defect sites. This sweeping action, combined with the unbalanced surface tension forces at the three-phase contact line, generates O-shaped ring structures composed of accumulated polymers, which ultimately fragment leading to the release of MNPs into the aquatic environment. Our findings demonstrate that microbubble-induced erosion represents a low-energy pathway for micropollutant release.

INTRODUCTION

Micro- and nanoplastics (MNPs) are globally emerging pollutants that threaten the environment, wildlife, and human health (*1*–*4*). The pervasive contamination of MNPs in aquatic environments has enabled their penetration into global food chains, with individuals now estimated to ingest up to 90,000 MNPs annually from bottled water alone (*5*). MNPs are characterized by their small particle size, strong adsorption capabilities, rapid migration, and pronounced accumulation rates in human tissue (*6*, *7*). Accumulation in carotid plaque is associated with increased risk of death or major cardiovascular events (*8*), while there are correlations between accumulation in brain tissue and neurodegenerative diseases (*6*, *7*). Understanding the mechanisms of MNP generation and release is critical to developing effective mitigation strategies. To date, most studies have focused on MNP release from bulk plastics in water environment due to factors such as mechanical wear and/or ultraviolet (UV) exposure (*9*–*11*). Despite the intimate contact between plastics and water in these environments, there is no fundamental understanding of how aquatic factors such as air bubbles, pH, and salt levels influence the generation of MNPs.

Air bubbles are pervasively found on the surfaces of plastics (*12*, *13*), particularly in daily-use items (e.g., plastic bottles) and on plastic debris along shorelines that are repeatedly exposed to air and water. Plastics have low surface energy, high hydrophobicity, and contain numerous surface imperfections, making them ideal for nucleating large quantities of air bubbles. Bubble nucleation results from the attraction of dissolved nonpolar air molecules to the hydrophobic plastic surface (*12*). The potential role of air bubbles in the transfer and release of MNPs has already attracted attention. Air bubbles can dislodge loose particles from the surfaces of plastics and carry them into the aquatic environment (*14*). Floating bubbles with MNPs attached act as vectors, facilitating the movement of MNPs within water columns (*15*–*17*). Small bubbles that remain adhered to the surfaces of MNPs can modify their physical properties, such as surface tension, zeta potential, and density, thereby altering MNPs' behavior, fate, and transport (*18*). MNP-coated bubbles that reach the water surface can burst and eject MNPs (typically <10 μm) into the atmosphere, substantially affecting the aerial distribution and transport of these pollutants (*17*, *19*).

Studies to date have focused on the potential of air bubbles to generate significant stresses at surfaces of plastics. The internal pressure within bubbles can reach 1 MPa (*20*, *21*), and when coupled with the levels of unbalanced stresses along the three phase contact line, substantial local deformation of the bulk plastic substrate becomes possible (*22*, *23*). Prior studies have shown that pressures of approximately 0.5 MPa can induce surface cracks in bottle containers (*14*, *24*). In principle, the pervasive presence of microbubbles in the water environment has the potential to erode and restructure the surfaces of plastics and drive the release of MNPs.

In this report, we studied the role of air bubbles [1 to 1000 μm of diameter (*25*)] in MNP generation on the surfaces of typical plastics. We investigated the nucleation, growth, and motion of microbubbles on polypropylene (PP) or polyethylene (PE), which account for 71% of MNPs found in the ocean (*26*), including their role in the erosion and accumulation of nascent MNPs on these plastics into O-shaped ring (OSR) structures. This behavior was observed on both standard and real-world plastic products across a wide temperature range (25° to 95°C) and in various water types [deionized

[1]Jiyang College, Zhejiang A&F University, Zhuji 311800, China. [2]AMBER Research Centre and Centre for Research on Adaptive Nanostructures and Nanodevices (CRANN), Trinity College Dublin, Dublin, Ireland. [3]Department of Civil, Structural and Environmental Engineering, Trinity College Dublin, Dublin, Ireland. [4]School of Chemical Sciences, RAPID Institute, Dublin City University, Dublin, Ireland. [5]School of Biological, Earth and Environmental Sciences, University College Cork, Cork, Ireland. [6]School of Chemistry, Trinity College Dublin, Dublin, Ireland. [7]TrinityHaus, Trinity College Dublin, Dublin, Ireland. [8]School of Civil Engineering, Sun Yat-Sen University, Guangzhou 510006, China. [9]Key Laboratory of Integrated Regulation and Resource Development on Shallow Lakes, Ministry of Education, College of Environment, Hohai University, Nanjing 210098, China. [10]Graduate Aerospace Laboratories and Department of Applied Physics, California Institute of Technology, Pasadena, CA, USA. [11]Huanjiang Laboratory, Zhejiang University, Zhuji, 311816, China.
*Corresponding author. Email: lidu@tcd.ie (D.L.); liwen.xiao@tcd.ie (L.X.); jjwang@tcd.ie (J.J.W.); jboland@tcd.ie (J.J.B.)

(DI) water, tap water, river water, and marine water]. OSR generation is a consequence of the unbalanced surface tension forces and shear stresses that exist at the water-bubble-plastic three-phase contact line. The edges of OSRs disintegrate piece by piece upon reexposure to water, while nascent MNPs remain intact at surface regions where bubble-induced erosion has not occurred. Raman spectroscopy, atomic force microscopy (AFM), diffusion-ordered spectroscopy (DOSY)–nuclear magnetic resonance (NMR), and scanning electron microscopy (SEM) identified the specific chemical and physical characteristics of MNPs released and traced them back to the disintegration of surface bound OSRs. Crucially, we demonstrate that microbubbles erode and restructure the surface morphology of plastics and promote the release of MNPs whenever plastics come into contact with water.

RESULTS

Characterization of microbubbles formed on the surface of plastics

We investigated the formation of microbubbles on plastic surfaces using an in situ observation chamber filled with water at adjustable temperatures (Fig. 1A). A standard PP sheet was submerged in the chamber (T_{water} = 25° to 95°C), and a high density of microbubbles formed within 1 min (Fig. 1, B to G). Top-view optical images

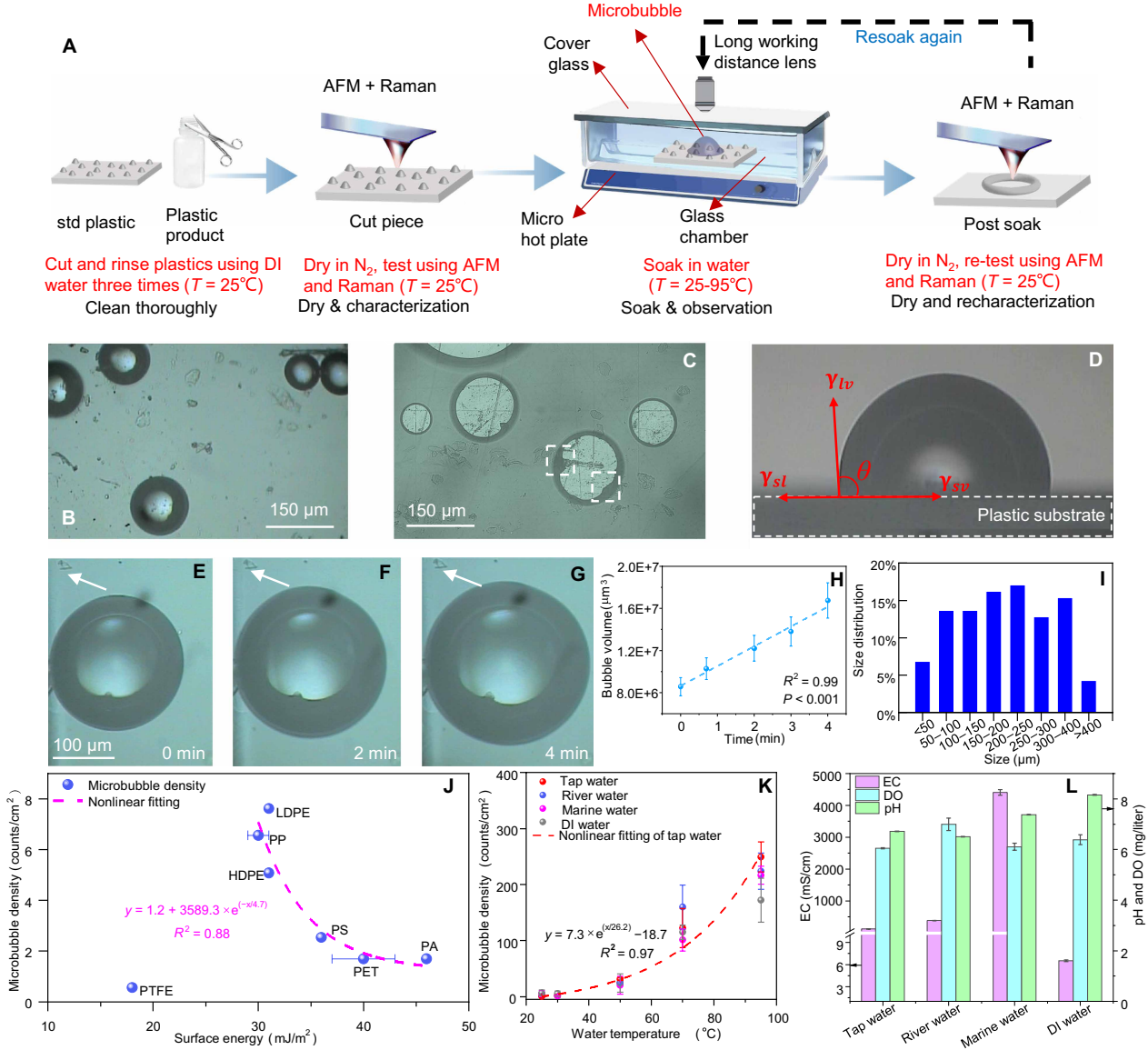

Fig. 1. Characterization of microbubbles on PP plastic surface. (**A**) Protocol used to characterize microbubbles in a glass chamber. (**B** to **D**) The top, bottom, and side view of typical microbubbles on PP surface in water, respectively. (**E** to **G**) The expansion process of microbubble over 4 min in 80°C water, observed from top. The white arrow indicates the same location. (**H**) The volume change of the observed microbubble shown in (E) to (G) over 4 min. (**I**) The diameter distribution of microbubbles formed on PP surface in water. (**J**) Correlation between plastic surface energy and microbubble density at 25°C. Surface energy values were obtained from 3M Company and previous research (*61*). PTFE was treated as an outlier and excluded from the fit. (**K**) Microbubble density in four common water types (tap water, river water, marine water, and DI water) at different temperatures (25° to 95°C). (**L**) Water quality characteristics of the four water types (n = 3 independent replicates per test).

(Fig. 1B) revealed dark outer circles at the edges of each bubble due to light refraction, with thicknesses ranging from approximately 20 to 100 μm, consistent with previous observations (*27*, *28*). Defects on the plastic substrate were seen most clearly in bottom-view images where they were frequently observed to pin and distort the contact line (white box, Fig. 1C). Side-view images showed a contact angle (θ) of 96.2° ± 2.2° (Fig. 1D), consistent with the known hydrophobic properties of PP plastics (*29*). Consequently, top-view images measure the outer bubble diameter, whereas bottom-view images capture the slightly smaller diameter at the contact line.

Top-view optical imaging was used to follow the dynamics of microbubble expansion and to capture their size distribution and density (Fig. 1, E to G). A typical microbubble in 80°C DI water, starting with a diameter of approximately 300 μm, expanded to about 375 μm after 2 min and reached 400 μm after 4 min. The linear increase in bubble volume with time is consistent with diffusion-based growth (Fig. 2H). Under steady-state condition (T_{water} = 80°C), a size distribution analysis (N = 117) showed that 20.5% were smaller than 100 μm, while a negligible fraction (less than 5%) of bubbles exceeded 400 μm in diameter (Fig. 1I). Microbubble formation and expansion was observed on all standard plastics including PP, low-density PE (LDPE), high-density PE (HDPE), PE terephthalate (PET), polyamide (PA), polystyrene (PS), and polytetrafluoroethylene (PTFE) as well as plastic samples submerged in various water types (DI water, tap water, river water, and marine water) at temperatures ranging from 25° to 95°C (Fig. 1, J and K, and fig. S1). A strong negative exponential correlation (R^2 = 0.88, PTFE is not included) was observed between surface energy and microbubble density (Fig. 2J) so that plastics with lower surface energy exhibit higher microbubble densities, consistent with reduced wettability that limits uniform

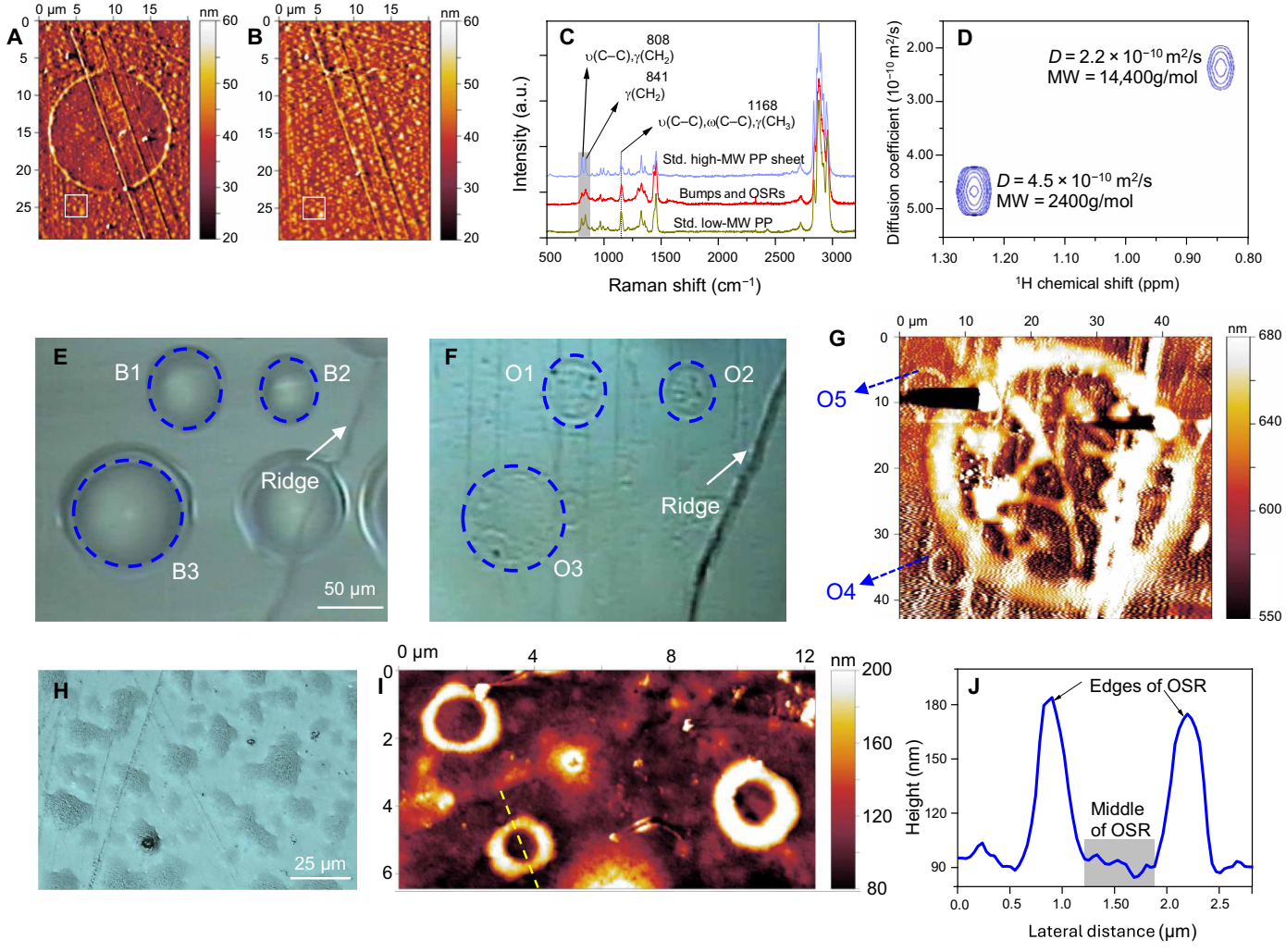

Fig. 2. Microbubble-induced erosion of PP surface to form OSRs. (**A**) AFM images of PP surface with migrated low-MW bumps. (**B**) The same location after soak in 50°C for 20 min. White boxes in (A) and (B) indicate the same region free of microbubble erosion before and after soak, respectively. (**C**) Raman spectra of standard PP sheet with relative high MW (97,000 g/mol), migrated low-MW bumps and OSRs from PP sheet surface and standard low-MW PP (3,700 g/mol). (**D**) ^{1}H 2D-DOSY spectrum of surface migrated low-MW bumps. (**E**) A typical optical image of microbubbles formed on PP surface soaked in 95°C water. (**F**) Optical image of the same location (see arrow marker) after N_2 dry. (**G**) AFM image of one typical OSR formed by the microbubble in (F). (**H**) Optical images of PE (low density) surface with migrated low-MW bumps. (**I**) AFM images of PE (low density) surface with migrated low-MW bumps after soak in 70°C water. (**J**) The extracted cross-sectional profiles of a typical OSR on (I) (indicated by the yellow dashed line). a.u., arbitrary unit.

water spreading and facilitates air entrapment promoting bubble formation (*30*). PTFE was the exception, which despite having the lowest surface energy, exhibited the lowest microbubble density, suggesting that surface chemistry or air adhesion properties are important. Temperature is also important. For typical waters (DI, tap, river, and marine water) with similar levels of dissolved oxygen (DO) and pH value, microbubble density on PP surfaces increased by approximately three orders of magnitude (around 0.5 to around 210 microbubbles per cm^2) as the temperature was increased from 25° to 95°C. A robust power-law relationship ($R^2 = 0.88$ to 0.7; see Fig. 1, K and L, and table S1) describes microbubble formation across this temperature range regardless of water type. Similar behaviors were found on other plastics. Despite vast differences in electrical conductivity microbubble densities in DI water and seawater were similar (Fig. 2K). Evidently, plastic type, temperature, DO levels, and pH values are key factors that regulate microbubble dynamics on plastic surfaces.

Microbubble-induced erosion of plastic surfaces and OSR formation

Microbubbles interact with defects that are pervasively found on the surface of plastics (Fig. 1C). Defects arise from environmental factors such as mechanical abrasion (*9*) and UV-induced cracks (*31*), or surface ridges and scratches introduced during manufacture (*32*) or even due to intrinsic stresses in the plastic itself that drive the migration of low molecular weight (MW) polymers or additives (*33*, *34*) to the plastic surface. Since stress-induced migration can be engineered precisely (see Materials and Methods), we used this approach to prepare plastic surfaces with controlled densities of surface defects. Specifically, we engineered standard PP plastic sheets (average MW 97,000) to trigger the migration of low-MW polymer to the plastic surface, thereby creating PP bumps at the surface with densities of 4 to 7 per 10 μm^2, and lateral sizes of 0.3 to 1 μm and heights of 7 to 10 nm (see Fig. 2A and Materials and Methods). Figure 2A shows the presence of surface ridges from the original manufacturing process, which serve as a marker of surface location. The PP sheet was placed in DI water at 25° to 50°C (typical environmental water temperature) and immediately nucleated microbubbles on the surface, resulting in the formation of OSRs (Fig. 2, A and B, and figs. S1 to S3). After 20 min in DI water at 50°C, the sheet was removed from the water and dried under nitrogen gas. AFM imaging of the same location in Fig. 2A showed the presence of a single OSR feature with a diameter of 15 μm (Fig. 2B). The height of the OSR's edge was around 30 nm, three to four times the height of the original surface bumps (7 to 10 nm). Within the OSR, there was a notable depletion in the density of PP bumps, while there was no substantial change in density outside the OSR (white box; Fig. 2, A and B). Large-area optical microscopy confirmed an OSR density of 32.2 ± 4.5 (around 10 cm^2, $n = 3$ independent replicates), with diameters spanning from tens to several hundred micrometers (fig. S2), consistent with the footprints of microbubbles attached to plastic surfaces. As a negative control, PP sheets were soaked in degassed water under otherwise identical conditions. No microbubbles or OSRs were observed (fig. S3). Evidently, OSRs are generated by microbubble nucleation and growth that erode PP bumps and accumulates them along the bubble's three-phase contact line (fig. S4). At the contact line, the horizontal component of the liquid-vapor surface tension, $\cos(\theta)\ \gamma_{lv}$, balances $\gamma_{sl} - \gamma_{sv}$ (*35*), whereas the vertical component, $\sin(\theta)\ \gamma_{lv}$, remains unbalanced and forces the accumulated PP upward to create the observed OSR. This unbalanced stress can reach 60 to 72 mN/m, depending on the temperature (25° to 95°C) (*36*) and is evidently sufficient to overcome the yield stress associated with low-MW PP.

Raman spectroscopy and DOSY (which is highly sensitive to low-MW polymer, Fig. 2, C and D) analysis confirmed that the bumps are predominantly low-MW PP (2400 to 14,400 g/mol) with low crystallinity. This is further evidenced by the substantially reduced intensity of the spectra at 810 and 1168 cm^{-1} recorded at these bumps, known to be associated with crystalline C–C backbone vibrations (*37*, *38*) that are present in semicrystalline bulk PP sheets (Fig. 2C) (*33*, *34*).

To investigate microbubble-induced erosion at elevated temperatures, a defective PP plastic piece with a high density of low-MW PP bumps was soaked in a glass chamber containing 95°C DI water (typical upper daily-use temperature). Large numbers of microbubbles immediately attached to the surface (Fig. 2E). After a 5-min soak, the PP piece was removed and dried using nitrogen gas. OSRs (O1 to O3 in Fig. 2F) were formed in the locations corresponding to the original microbubbles B1, B2, and B3 (Fig. 2E). Two particles were observed within the OSR induced by microbubble B1, suggesting these particles may have facilitated microbubble nucleation. AFM imaging of the OSR at B1 captured these pinning particles and showed that in addition to the largest ring, there were many small OSRs (O4 and O5 in Fig. 2G) and residues of OSR features both within and outside the largest OSR induced by microbubble B1. Evidently, smaller microbubbles formed in the same location before the formation of B1, consistent with large microbubble densities at elevated water temperatures (Fig. 1K).

OSRs were observed on defective PP plastic sheets following exposure to room temperature (25°C) water from three environmental sources (tap water, river water, and marine water). In addition to OSRs, particle growth, likely salt crystals, was observed in the marine water sample, indicating that water composition may influence the formation of OSRs (fig. S5C). In contrast to the higher-temperature water conditions (Fig. 2, F and G), the OSRs formed at room temperature were singular, without overlapping or residual OSRs (fig. S5), consistent with the lower microbubble density and slower dynamics of microbubbles at room temperature.

LDPE sheets tested using the same protocol (Fig. 1A) also exhibited numerous OSRs (Fig. 2, H and I). The average OSR diameter on PE surfaces was only 2.2 ± 0.4 μm, much smaller than that on PP, where most OSRs were larger than 15 μm (Fig. 2, B and F). AFM cross-sectional profiles of these OSRs revealed edge thicknesses of 80 to 120 nm (Fig. 2I), significantly larger than those on PP surfaces (Fig. 2B). Evidently polymer material properties influence both bubble nucleation and subsequent surface restructuring, in this case most likely due to the lower glass transition temperature (Tg) and hence lower yield stress of PE compared to PP.

Disintegration of OSRs formed by microbubbles

Plastic products always contain surface defects and high levels of residual stress so that it is not necessary to stress engineer bump-like defects. A piece of PP sheet from a brand-new plastic bottle was analyzed by AFM. Figure 3 (A and B) showed the original surface topography and the corresponding phase image, respectively. Surface ridges and scratches evident in the topography image, shows no contrast in the phase image, consistent with a surface of uniform modulus or stiffness. The PP sheet was then soaked in 95°C DI water within a glass chamber [consistent with EU Regulation 2020/1245 for any plastic-contact condition exceeding 40°C (*39*)—a scenario

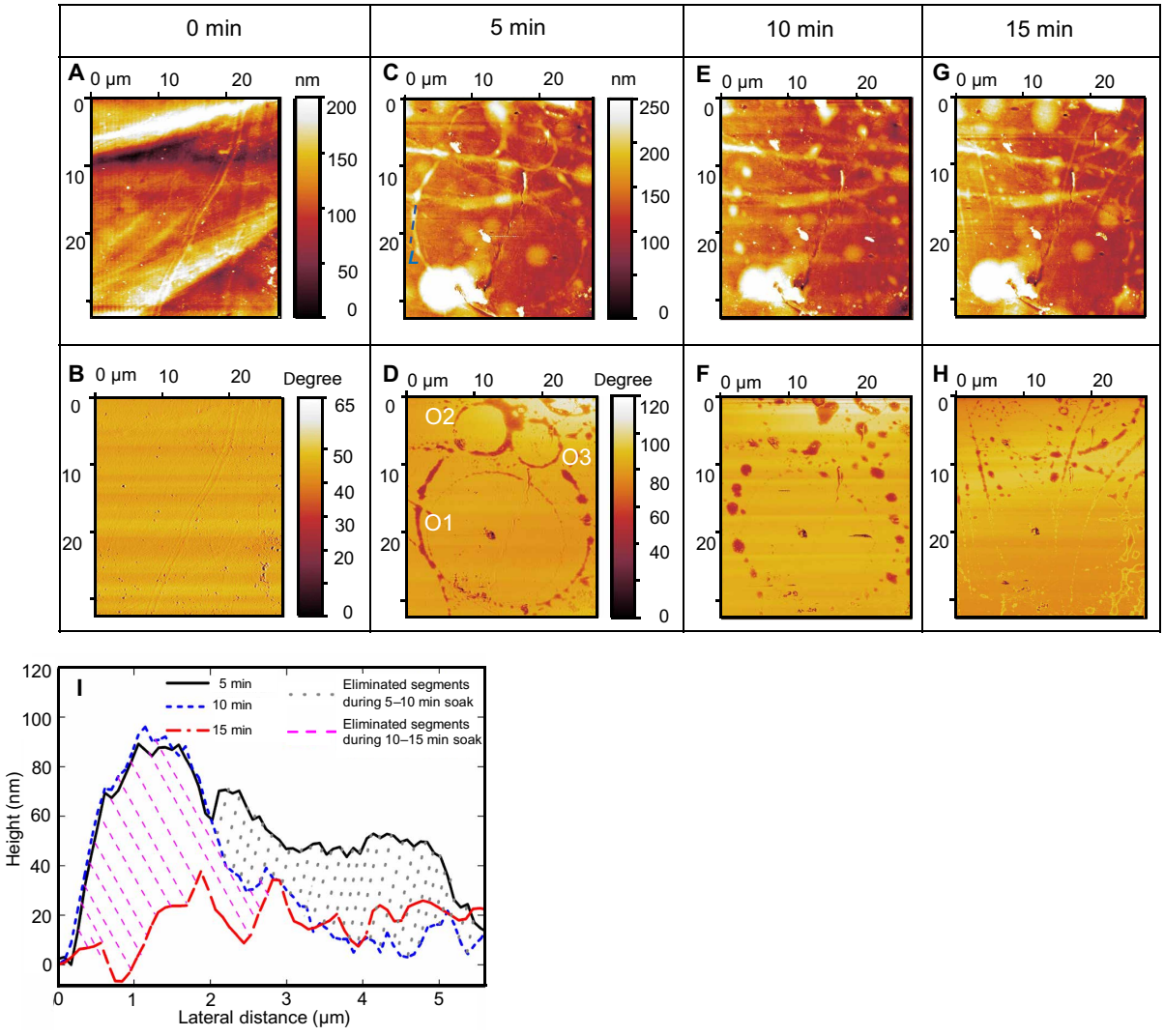

Fig. 3. Disintegration of OSR on PP bottle surface when soaked in hot water (95°C) revealed by AFM images. The upper images (**A**, **C**, **E**, and **G**) were the height change of PP bottle surface, while the lower set (**B**, **D**, **F**, and **H**) showed the corresponding phase image change. Images [(A) and (B)] showed the height and phase images of typical PP surface without O rings before being soaked into hot water, respectively. After 5 min of soaking into hot water, we observed the O rings forming on some parts of the PP surface. Focusing on the O rings, it was found the rings broke down piece by piece and disappeared eventually with soaking time increase [height change from (C) to (E) and (G); phase change from (D) to (F) and (H)]. [(C), (E), and (G)] shared the same color scale bar in (C). The color scale bar in (C) indicates the height; [(D), (F), and (H)] shared the same color scale bar in (D). The color scale bar in (D) indicates the angle of phase image. (I) demonstrated the cross-sectional profiles extracted from the blue line *L* in [(C), (E), and (G)].

commonly encountered in plastic coffee cups and microwavable containers] and a large quantity of microbubbles formed on the surface immediately. After 5 min, the PP piece was removed and dried with nitrogen gas, examined by AFM (Fig. 3, C and D), and revealed the presence of the OSRs. The phase image (Fig. 3D) now shows significant contrast between the plastic surface and the OSRs, consistent with a reduced stiffness of the material the makes up the latter. Raman spectroscopy confirmed that the material that comprised the OSRs was low-MW polymers (see Fig. 4D), indicating that the migration of low-MW polymer from defects is a pervasive recovery phenomenon in plastics, which was subsequently eroded and restructured by microbubbles to form the observed OSRs.

After the PP piece was soaked for a second time for 5 min in 95°C water and dried with nitrogen gas, the edge of OSR O1 (Fig. 3D) broke into small pieces, while most of the edges of O2 and O3 had disappeared. Repeating the soak process for an additional 5 min resulted in the complete disappearance of all three OSRs. AFM cross-sectional analysis along a typical OSR edge (marker L in Fig. 3C) showed that the first 5-min soak transformed the continuous edge into a series of droplets of similar sizes (Fig. 3, C to F), which is likely attributable to Plateau-Rayleigh instability in the low-MW viscoelastic material (*40*). The broken segments were approximately 2 to 3 μm in length and 20 to 60 nm in height (Fig. 3I). The cross section revealed that the eliminated OSR segments had lengths of about 3 μm and heights of around 40 nm. During the 5- to 10-min soak, the eliminated segments had similar lengths but with increased heights of around 60 nm. There was no evidence that material removed from the OSRs relocated or attached elsewhere—consistent

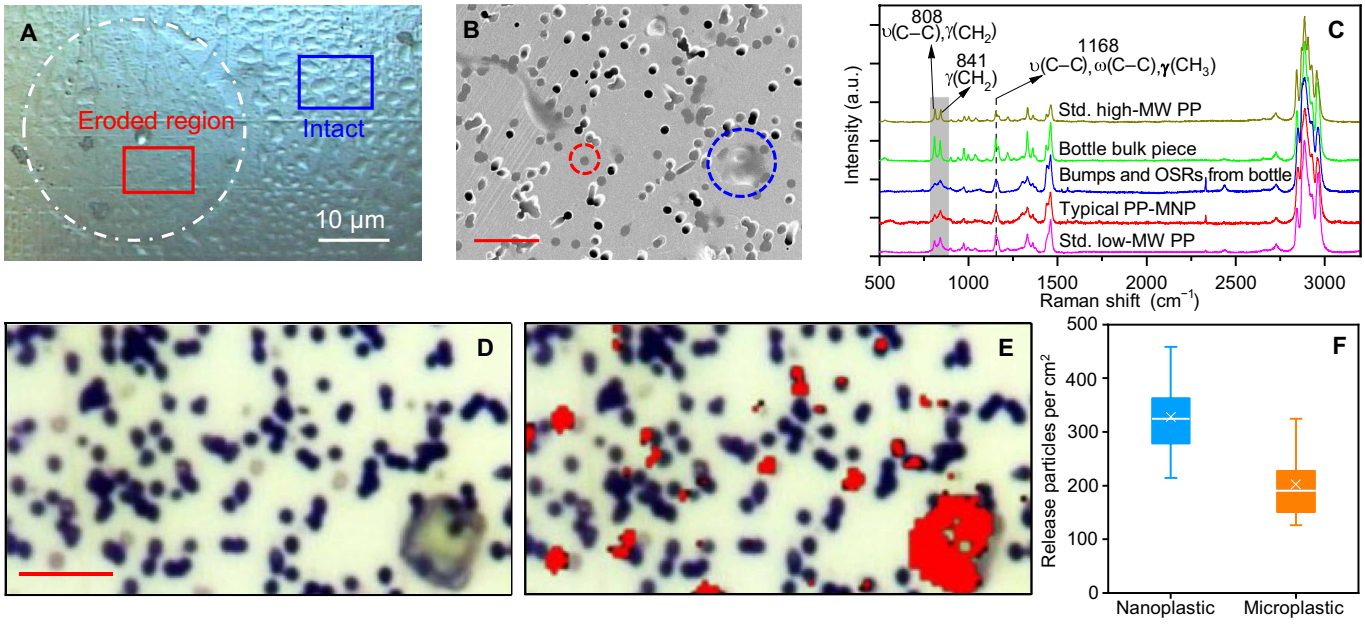

Fig. 4. PP MNP release from PP bottle. (**A**) Typical optical image of PP surface after hot water exposure. Blue box area has high quantity of intact bumps, while the red box showed bumps deformed by a microbubble at the hot water-PP plastic interface. An OSR was also formed. (**B**) SEM image of typical PP microplastic (blue circle) and nanoplastic (red circle) captured on membrane filter surface (800-nm pore size). (**C**) Raman spectra of inner surface of bulk PP bottle, PP bumps, and OSRs from the inner surface of PP after exposure, captured nanoplastic from exposed water, standard high-MW PP (97,000 g/mol), and standard low-MW PP (3700 g/mol), respectively. (**D**) Optical image of the released particles captured on membrane filter surface. (**E**) Raman mapping and identification of captured PP particles in (B). (**F**) MNPs released from unit area of PP bottle during hot water exposure. The red scale bar in [(B) and (D)] is 5 μm.

with observations on standard PP sheets (Fig. 2, A and B) and whole bottles (Fig. 4B). The compressive stress at the surface of plastics makes it unlikely that low-MW polymers are reabsorbed into the bulk plastic (*33*, *34*). Evidently, the material from the breakup of OSRs is released into the water, thereby increasing the level of MNPs in the environment.

MNP release driven by microbubbles

The levels of MNPs released via microbubbles was measured. A brand-new PP bottle (average-MW 64,000, typical medium-MW PP, fig. S6) was filled with 95°C hot water and placed in a 95°C DI water bath for 4 hours following a standard protocol [EU Regulation 2020/1245 for any plastic-contact condition exceeding 40°C (*39*)] detailed in fig. S7. Large numbers of microbubbles immediately appeared on the inner surface of the bottle, consistent with our in situ observations on standard plastic sheets (Fig. 1 and fig. S1). Postexposure optical images showed that some areas of the inner PP surface (Fig. 4A, blue box) contained large numbers of bumps similar to those found on standard PP sheets, while in other areas, the bumps were deformed into OSRs by microbubbles formed during the soak (Fig. 4B). Few bumps were observed within the OSRs (Fig. 4A, red box) consistent with the material being swept along at the bubbles' three-phase contact line, as discussed earlier (Fig. 2B).

After the 4 hours of soaking period, an analysis of the water within the bottle revealed that per cm^2 of the bottle's interior surface 202 ± 62 PP microplastics (≥1 μm) and 328 ± 62 PP nanoplastics (800 to 1000 nm) were released, respectively (Fig. 4, B to F). Nanoplastics below 800 nm were not captured in this analysis. Ethanol pretreatment was used to eliminate interference from additives (*41*) and oligomers (*4*) that might also be released into the water. Raman spectra revealed that most MNPs closely matched the spectrum for standard low-MW PP with low crystallinity (hit quality index, HQI = 0.93), whereas clear differences were observed between MNPs and the PP bottle (HQI of only 0.75, Fig. 4C; for details, see Supplementary Text). Notably, the Raman spectra of surface-segregated bumps/OSRs and MNPs showed that they were nearly identical (HQI of 0.98). Membrane-captured MNPs were soft and gel-like, consistent with the reduced stiffness found in AFM, and with lateral sizes around 0.8 to 5 μm (Fig. 4, B to F) that closely matched the sizes of the eliminated sections of the OSRs in Fig. 3I. The close correspondence in the physicochemical properties of the captured MNPs and OSRs confirms that microbubbles are a major factor in the erosion of plastics surfaces and the release of MNPs into water.

DISCUSSION

In this study, we identified the pervasive formation of microbubbles on plastic surfaces as a critical, yet previously overlooked, mechanism for MNP release from bulk plastics. Microbubble-induced erosion of plastic surfaces occurs independently and in parallel with bulk mechanical breakdown or the UV-induced oxidative degradation. UV photodegradation demands a sustained flux of high-energy photons—months to years of sunlight or energy-intensive laboratory lamps—to cleave polymer bonds (*42*). Mechanical abrasion, whether from waves, sand, industrial grinding, or turbulent mixers, must supply enough external work to overcome the polymer's fracture toughness (*43*, *44*). In contrast, microbubbles nucleate spontaneously whenever water conditions allow, requiring no mechanical agitation or radiant power. The bubble's surface tension provides the

localized micro-Newton forces that peel low-MW material from defects; thus, the energy that drives fragmentation is drawn directly from the interfacial free energy already present in the system. Consequently, microbubble-induced OSR fragmentation constitutes a genuinely low-energy pathway for MNP release, which operates wherever water and plastic surfaces come into contact.

Microbubble formation depends jointly on the exposed water quality and the physicochemical properties of plastic surfaces (*45*). Reduced gas solubility in water at elevated temperatures increases gas supersaturation levels and drives bubble nucleation and growth on plastic surfaces (*46*). This phenomenon is reflected by the exponential increase in bubble density observed at higher temperatures across various water types (Fig. 1K). Similarly, increased DO levels (e.g., from shaking/aeration) and lower salinity (higher gas solubility) provide additional dissolved gas for bubble formation (*47*). Conversely, lowering DO levels causes existing microbubbles to shrink and dissolve by diffusion, as predicted by Epstein-Plesset theory (*48*) and supported by microbubble-dissolution tests (fig. S8). Surface properties and heterogeneity also regulate bubble nucleation. Hydrophobic polymers, such as PP and PE, have inherent surface defects, and are particularly prone to facilitating bubble formation due to enhanced gas entrapment (Fig. 1J). Intrinsic stresses and chemical incompatibility drive the expulsion of low-MW substances like plastic additives and amorphous polymers to the surface under typical use conditions (*33*, *34*, *49*). In addition, environmental surface cracking (straight, branched or spider-web-like) creates channels that both trap air (*31*) and facilitate low-MW substances migration from bulk plastic to surface, further amplifying microbubble-based surface erosion. Notably, in natural waters and daily use settings, surface morphology evolves over time [e.g., biofilm growth (*50*), particle deposition (*51*), or coated with passivation layers (*52*)], which can increase surface energy, reduce hydrophobicity, and compete for nucleation sites, thereby modulating microbubble formation and attachment. Resolving these competing effects will require systematic studies using the protocols established in this study.

Bubble-induced surface erosion facilitates the release of MNPs. Our results show a distinct difference between the levels of MNPs released from bubble-induced OSRs compared to pristine bumps on bubble-free regions of the surface. Pristine protrusions remain predominantly intact under static immersion or mild hydrodynamic conditions (Figs. 2B and 4B), whereas those that are eroded and restructured into OSRs by microbubbles readily disintegrate and are released as MNPs into the surrounding water (Fig. 3, C to H). This distinction arises because original surface protrusions remain mechanically interlocked with microstructures on the plastic surface (*33*, *34*), providing stability against detachment. Bubble dynamics, including capillary-driven movement and the unbalanced upward stresses, disrupt this micromechanical interlocking or may even induce polymer chain scission (*22*, *23*), facilitating accumulation and formation of OSRs and increasing the levels of MNP release. Temperature critically modulates bubble-induced restructuring, and consequently, MNP release. At room temperature, the increased mechanical stiffness of the surface bumps pins microbubbles for longer, allowing them to sweep up more low-MW material and build rims that are both wider and taller than those produced at 50°C (Fig. 2B and fig. S9; Supplementary cross sections). Although these taller rims should in principle be more vulnerable to hydrodynamic shear, their increased stiffness slows Plateau-Rayleigh breakup of the viscoelastic matrix (Fig. 3), delaying necking and detachment (*40*). Hence, OSR fragmentation under ambient conditions—and the attendant release of MNPs—proceeds over much longer timescales than at elevated temperatures. Consistent with this, water-land interfaces (e.g., beaches), which often experience higher temperatures, are widely reported as dominant hotspots for MNP fragmentation, whereas fragmentation in the open ocean is generally slower and contributes less (*53*, *54*). Our tests also revealed that microbubbles formed on surfaces can restructure additive particles, generating additive-rich OSRs (fig. S10). This suggests that microbubbles may simultaneously promote the release of plastic additives and microplastics, enhancing their mutual attachment and consequently increasing environmental and health risks (*55*).

Despite recent attention to bubble-mediated MNP transport and emission (*15*, *19*), most studies have focused on MNP release from bulk plastics due to nonaquatic factors such as mechanical wear or UV exposure (*9*–*11*). We have demonstrated that aquatic microbubbles that pervasively form on plastic surfaces can induce microscale erosion and promote MNP generation whenever plastics come into contact with water. A continuum perspective is warranted. Although nanobubbles are unlikely to account for the microscale surface erosion and OSRs reported here, they may still induce nanoscale surface erosion and release tens-of-nanometer–sized MNPs via high Laplace pressure and unbalanced contact-line stresses—a release size regime that is more mobile and potentially more toxic (*18*, *22*) but beyond the scope of the present study. By tuning environmental parameters (e.g., water types, exposure temperature, DO, salinity, and UV exposure) and plastic properties (e.g., plastic types, surface defects, biofilm attached, MW, and crystallinity degree), researchers can systematically explore the impact of bubble size (especially nanobubbles), contact angle, gas composition, lifetime, and bubble-substrate interactions on OSR generation and MNP release. We anticipate that our findings will prompt further studies on the role of aquatic factors and the development of strategies (from surface coatings and materials modification to water-quality control) to mitigate the release of plastic pollutants.

MATERIALS AND METHODS

Characterization of microbubbles formed on the surface of plastics

To investigate how microbubbles form on plastic surfaces in aquatic environments, we used an in situ observation chamber filled with water at adjustable temperatures (Fig. 1A). The glass chamber measured 5 mm in depth, 60 mm in length, and 35 mm in width and was placed on a micro hot plate (PTC Aluminum Shell Ceramic Heating Plate) to maintain the desired temperature. A piece of standard PP sheet (Goodfellow, typically 30 mm by 15 mm, 0.5-mm thickness) was placed to the middle of the chamber using waterproof double-sided tape (1-mm thickness) fixed two ends. DI water was preheated in a thermal bath to the required temperature (25° to 95°C depending on the experiment) then poured into the chamber; a cover glass was placed on top and the hot plate was used to sustain the set temperature. Immediately after setup the microbubbles on the top and bottom surfaces (focusing through the transparent plastic sheet) of the plastic sheet (in its central region) were observed under an optical microscope (Olympus BX 53 M equipped with a Mitutoyo M Plan Apo 100× lens). To measure the contact angle of the microbubbles on the plastic surface, we replaced the plastic sample with a 30 mm–by–2 mm strip and rotated it 90° to obtain a side view. To

determine how different plastics affect microbubble formation, we tested various standard plastic sheets (LDPE from Alfa Aesar; HDPE, PA, PET, PP, PS, and PTFE from Goodfellow) following the same protocol. To evaluate how typical water sources affect microbubble formation, we collected tap water (from Zhejiang A&F University, Zhejiang, China), freshwater (Yangtze River, Jiangsu, China), and marine water (South China Sea, Guangdong, China). These replaced DI water under the same experimental procedure. Microbubble characteristics (size, density, and contact angle) were analyzed using ImageJ (version 1.53a).

Microbubble-induced erosion of plastic surfaces to form OSRs

Standard PP sheets and stainless-steel O-rings were thoroughly rinsed with DI water (three times at room temperature). Each PP sheet was rolled into a cylindrical shape (diameter ~40 mm) using a stainless-steel O-ring and placed in a 95°C oven for 4 hours to generate controlled densities of surface defects (migrated low MW bumps). The treated PP cylinder was then placed on a clean glass plate to cool. After cooling, the PP cylinder was carefully cut for surface analysis using optical microscopy, AFM, Raman spectroscopy, and Fourier transform infrared (FTIR). The cut piece was then soaked in the observation chamber (described above) filled with DI water at different temperatures (50°C for 20 min, 95°C for 5 min). After soaking, the PP sheet was removed, dried with nitrogen gas, and inspected under optical microscopy and AFM. As a negative control, PP pieces were also soaked in degassed DI water. Following an established protocol (*56*), degassed water was prepared by boiling DI water in a glass beaker, sealing with a cap, and cooling to room temperature for later use. To examine how different water sources affect microbubble-induced surface erosion, we used the same procedure but replaced DI water with tap water (Trinity College Dublin, Ireland and Zhejiang A&F University, Zhuji, China), freshwater (River Liffey, Dublin, Ireland and Yangtze River, Nanjing, China), or marine water (East China Sea) when testing PP sheets with surface defects. A raw PP sheet with fewer defects served as the control. To investigate the chemical properties of the migrated defects, we separated the heat-induced bumps on the plastic sheet using aluminium foil. Following established protocols, we used Raman spectroscopy (Renishaw InVia) (*41*) and DOSY (*57*) to determine chemical composition and MW, respectively. The Raman spectrometer (532 nm laser, Coherent Inc.) was equipped with a cooled charge-coupled device and a microscope (NT-MDT) with a 100× objective (Mitutoyo, M Plan Apo). System calibration was performed before each sample test by verifying the silicon wafer peak at 520.7 cm^{-1} (>6000 counts for a 1-s exposure, 1 accumulation, ~180 μW laser on the sample). Following established methods (*41*, *58*), typical MNP measurements used 10-s exposures with three accumulations over the 250 to 3500 cm^{-1} range. Spectra were processed in WiRE 3.4 (Renishaw) with an HQI threshold of 0.7 for MNP identification; background subtraction was performed if necessary (*41*). To measure the MW of the separated bumps, we dissolved them in $CDCl_3$ and conducted ^1H DOSY NMR (Bruker AVANCE, 256 scans), which is sensitive to low-MW polymers. Surface topography of the plastic was analyzed with an NT-MDT AFM (Nova NT-MDT SPM software), and the resulting AFM data for migrated defects and OSRs were processed in Gwyddion 2.54.

Disintegration of OSRs formed by microbubbles on a real plastic bottle

Plastic products generally have manufacturing defects and high residual stress, so it was unnecessary to use the stress-engineering process described earlier to create bump-like defects. To test this, a PP sheet cut from a brand-new plastic bottle was thoroughly cleaned with DI water and initially characterized under AFM. The sheet was then soaked in 95°C DI water in the glass chamber (consistent with EU Regulation 2020/1245 for any plastic-contact condition exceeding 40°C (*39*), a scenario common in plastic bottles and containers for food). After 5 min, the PP piece was removed from the water, dried with nitrogen gas, and examined by AFM (Fig. 3, C and D), revealing OSRs. We then focused on the same surface location containing three OSRs (Fig. 3, C and D), soaked the PP piece again in 95°C water for 5 min and dried it with nitrogen gas. This process was repeated three times until most of the OSR edges disappeared.

MNP release driven by microbubbles

Precautions to prevent sample contamination

All hardware and plastic samples were washed and thoroughly rinsed with room-temperature DI water to minimize contamination. Before sample preparation, the cleaned hardware and samples were kept in a clean glass container. Throughout sample preparation and testing, particle-free nitrile gloves and 100% cotton laboratory coats were used. Coat sleeves were secured inside the nitrile gloves, and both gloves and sleeves were rinsed with distilled water followed by DI water before every procedure. All equipment that made contact with the samples was fabricated from clean borosilicate glass 3.3. Glassware used for sample filtration and storage (e.g., glass filter holders and glass petri dishes) was also extensively cleaned with DI water. The DI water was obtained from a Veolia UltraPure water system coupled with a Thermo Fisher Scientific Barnstead Nanopure unit fitted with a 0.2-μm absolute final filter to dispense and monitor water quality (conductivity of 1.5 μs/cm and resistivity of 18.2 MΩ). Control experiments (Fig. 3A) using only DI water and glass beakers without plastic samples did not detect any PP MNPs, confirming the reliability of this approach.

MNP release from PP bottles

The potential for MNP release from PP bottles was studied following the protocol illustrated in Fig. 4A. New PP bottles were rinsed three times with room-temperature DI water, and then each bottle was filled with 95°C DI water and immersed in a 95°C water bath for 4 hours. Afterward, the bottles were placed on a clean glass plate and allowed to cool. The water in each bottle was then gently shaken and passed through a gold-coated polycarbonate membrane filter (25 mm diameter, 0.8-μm pore size, APC) commonly used in MNP studies (*59*, *60*). Next, 20 ml of ethanol, which has negligible effects on the morphology of typical plastics and MNPs, was also filtered to remove any remaining plastic additives, facilitating MNP identification (*41*). The membrane filter was carefully transferred to a clean cover glass and stored in a clean glass petri dish (Brand, Thermo Fisher Scientific). The captured particles were characterized with Raman spectroscopy, FTIR, AFM, and SEM. Afterward, small pieces were cut from the soaked bottles for AFM, SEM, Raman, and FTIR analyses to examine the surface morphology and any chemical changes. To investigate MNP release from the bottle body, the water volume was lowered, so the inner surfaces of neck and mouth did not

come in contact with the water surface; the bottle was then examined using optical microscope, Raman spectroscopy, AFM, and SEM.

Supplementary Materials

This PDF file includes:

Supplementary Text
Figs. S1 to S10
Table S1

REFERENCES

1. A. D. Vethaak, J. Legler, Microplastics and human health. *Science* **371**, 672–674 (2021).
2. Y. Feng, C. Tu, R. Li, D. Wu, J. Yang, Y. Xia, W. J. G. M. Peijnenburg, Y. Luo, A systematic review of the impacts of exposure to micro-and nano-plastics on human tissue accumulation and health. *Eco Environ. Health* **2**, 195–207 (2023).
3. V. Nava, S. Chandra, J. Aherne, M. B. Alfonso, A. M. Antão-Geraldes, K. Attermeyer, R. Bao, M. Bartrons, S. A. Berger, M. Biernaczyk, R. Bissen, J. D. Brookes, D. Brown, M. Cañedo-Argüelles, M. Canle, C. Capelli, R. Carballeira, J. L. Cereijo, S. Chawchai, S. T. Christensen, K. S. Christoffersen, E. de Eyto, J. Delgado, T. N. Dornan, J. P. Doubek, J. Dusaucy, O. Erina, Z. Ersoy, H. Feuchtmayr, M. L. Frezzotti, S. Galafassi, D. Gateuille, V. Gonçalves, H.-P. Grossart, D. P. Hamilton, T. D. Harris, K. Kangur, G. B. Kankılıç, R. Kessler, C. Kiel, E. M. Krynak, À. Leiva-Presa, F. Lepori, M. G. Matias, S.-I. S. Matsuzaki, Y. M. Elarney, B. Messyasz, M. Mitchell, M. C. Mlambo, S. N. Motitsoe, S. Nandini, V. Orlandi, C. Owens, D. Özkundakci, S. Pinnow, A. Pociecha, P. M. Raposeiro, E.-I. Rõõm, F. Rotta, N. Salmaso, S. S. S. Sarma, D. Sartirana, F. Scordo, C. Sibomana, D. Siewert, K. Stepanowska, Ü. N. Tavşanoğlu, M. Tereshina, J. Thompson, M. Tolotti, A. Valois, P. Verburg, B. Welsh, B. Wesolek, G. A. Weyhenmeyer, N. Wu, E. Zawisza, L. Zink, B. Leoni, Plastic debris in lakes and reservoirs. *Nature* **619**, 317–322 (2023).
4. T. Yang, Y. Xu, G. Liu, B. Nowack, Oligomers are a major fraction of the released submicrometre particles released during washing of polyester textiles. *Nat. Water* **2**, 151–160 (2024).
5. K. D. Cox, G. A. Covernton, H. L. Davies, J. F. Dower, F. Juanes, S. E. Dudas, Human consumption of microplastics. *Environ. Sci. Technol.* **53**, 7068–7074 (2019).
6. F. Dang, Q. Wang, Y. Huang, Y. Wang, B. Xing, Key knowledge gaps for One Health approach to mitigate nanoplastic risks. *Eco Environ. Health* **1**, 11–22 (2022).
7. A. J. Nihart, M. A. Garcia, E. El Hayek, R. Liu, M. Olewine, J. D. Kingston, E. F. Castillo, R. R. Gullapalli, T. Howard, B. Bleske, J. Scott, J. Gonzalez-Estrella, J. M. Gross, M. Spilde, N. L. Adolphi, D. F. Gallego, H. S. Jarrell, G. Dvorscak, M. E. Zuluaga-Ruiz, A. B. West, M. J. Campen, Bioaccumulation of microplastics in decedent human brains. *Nat. Med.* **31**, 1114–1119 (2025).
8. R. Marfella, F. Prattichizzo, C. Sardu, G. Fulgenzi, L. Graciotti, T. Spadoni, N. D. Onofrio, L. Scisciola, R. La Grotta, C. Frigé, V. Pellegrini, M. Municinò, M. Siniscalchi, F. Spinetti, G. Vigliotti, C. Vecchione, A. Carrizzo, G. Accarino, A. Squillante, G. Spaziano, D. Mirra, R. Esposito, S. Altieri, G. Falco, A. Fenti, S. Galoppo, S. Canzano, F. C. Sasso, G. Matacchione, F. Olivieri, F. Ferraraccio, I. Panarese, P. Paolisso, E. Barbato, C. Lubritto, M. L. Balestrieri, C. Mauro, A. E. Caballero, S. Rajagopalan, A. Ceriello, B. D. Agostino, P. Iovino, G. Paolisso, Microplastics and nanoplastics in atheromas and cardiovascular events. *N. Engl. J. Med.* **390**, 900–910 (2024).
9. A. L. Andrady, The plastic in microplastics: A review. *Mar. Pollut. Bull.* **119**, 12–22 (2017).
10. Y. Shi, L. Zheng, H. Huang, Y.-C. Tian, Z. Gong, P. Liu, X. Wu, W.-T. Li, S. Gao, Formation of nano-and microplastics and dissolved chemicals during photodegradation of polyester base fabrics with polyurethane coating. *Environ. Sci. Technol.* **57**, 1894–1906 (2023).
11. Y. K. Song, S. H. Hong, M. Jang, G. M. Han, S. W. Jung, W. J. Shim, Combined effects of UV exposure duration and mechanical abrasion on microplastic fragmentation by polymer type. *Environ. Sci. Technol.* **51**, 4368–4376 (2017).
12. D. J. Wesley, R. M. Smith, W. B. Zimmerman, J. R. Howse, Influence of surface wettability on microbubble formation. *Langmuir* **32**, 1269–1278 (2016).
13. Y. Shen, L. Hu, W. Chen, H. Xie, X. Fu, Drop encapsulated in bubble: A new encapsulation structure. *Phys. Rev. Lett.* **120**, 054503 (2018).
14. Y. Chen, H. Xu, Y. Luo, Y. Ding, J. Huang, H. Wu, J. Han, L. Du, A. Kang, M. Jia, W. Xiong, Z. Yang, Plastic bottles for chilled carbonated beverages as a source of microplastics and nanoplastics. *Water Res.* **242**, 120243 (2023).
15. S. Moon, L. M. A. Martin, S. Kim, Q. Zhang, R. Zhang, W. Xu, T. Luo, Direct observation and identification of nanoplastics in ocean water. *Sci. Adv.* **10**, eadh1675 (2024).
16. H. Jiang, J. Bu, K. Bian, J. Su, Z. Wang, H. Sun, H. Wang, Y. Zhang, C. Wang, Surface change of microplastics in aquatic environment and the removal by froth flotation assisted with cationic and anionic surfactants. *Water Res.* **233**, 119794 (2023).
17. R.-F. Shiu, L.-Y. Chen, H.-J. Lee, G.-C. Gong, C. Lee, New insights into the role of marine plastic-gels in microplastic transfer from water to the atmosphere via bubble bursting. *Water Res.* **222**, 118856 (2022).
18. Z. Wang, C. An, K. Lee, Q. Feng, Overlooked role of bulk nanobubbles in the alteration and motion of microplastics in the ocean environment. *Environ. Sci. Technol.* **57**, 11289–11299 (2023).
19. S. Allen, D. Allen, V. R. Phoenix, G. Le Roux, P. D. Jiménez, A. Simonneau, S. Binet, D. Galop, Atmospheric transport and deposition of microplastics in a remote mountain catchment. *Nat. Geosci.* **12**, 339–344 (2019).
20. Y. Sun, G. Xie, Y. Peng, W. Xia, J. Sha, Stability theories of nanobubbles at solid-liquid interface: A review. *Colloids Surf. A* **495**, 176–186 (2016).
21. S. Khuntia, S. K. Majumder, P. Ghosh, Microbubble-aided water and wastewater purification: A review. *Rev. Chem. Eng.* **28**, 191–221 (2012).
22. S. Ren, C. Pedersen, A. Carlson, T. Salez, Y. Wang, Capillary deformation of ultrathin glassy polymer films by air nanobubbles. *Phys. Rev. Res.* **2**, 043166 (2020).
23. Y. Wang, B. Bhushan, X. Zhao, Nanoindents produced by nanobubbles on ultrathin polystyrene films in water. *Nanotechnology* **20**, 045301 (2009).
24. G. Xie, Z. Yin, L. Wang, Z. Hu, C. Zhu, Effects of gas pressure on the failure characteristics of coal. *Rock Mech. Rock Eng.* **50**, 1711–1723 (2017).
25. T. Bodnár, G. P. Galdi, Š. Nečasová, *Particles in Flows* (Springer, 2017).
26. M. N. Issac, B. Kandasubramanian, Effect of microplastics in water and aquatic systems. *Environ. Sci. Pollut. Res.* **28**, 19544–19562 (2021).
27. S. Patra, D. K. Bal, S. Ganguly, Diffusion of moisture from hydrogel scaffold with induced porosity from self-assembled bubbles. *Drying Technol.* **33**, 336–345 (2015).
28. M. Sumikura, M. Hidaka, H. Murakami, Y. Nobutomo, T. Murakami, Ozone micro-bubble disinfection method for wastewater reuse system. *Water Sci. Technol.* **56**, 53–61 (2007).
29. K. Min, J. D. Cuiffi, R. T. Mathers, Ranking environmental degradation trends of plastic marine debris based on physical properties and molecular structure. *Nat. Commun.* **11**, 727 (2020).
30. S. T. Yohe, J. D. Freedman, E. J. Falde, Y. L. Colson, M. W. Grinstaff, A mechanistic study of wetting superhydrophobic porous 3D meshes. *Adv. Funct. Mater.* **23**, 3628–3637 (2013).
31. H. Deng, L. Su, Y. Zheng, F. Du, Q.-X. Liu, J. Zheng, Z. Zhou, H. Shi, Crack patterns of environmental plastic fragments. *Environ. Sci. Technol.* **56**, 6399–6414 (2022).
32. Q. Liang, W. Zhu, W. Sun, Z. Yu, Y. Wang, D. Zhang, In-line inspection solution for codes on complex backgrounds for the plastic container industry. *Measurement* **148**, 106965 (2019).
33. K. Bhunia, S. S. Sablani, J. Tang, B. Rasco, Migration of chemical compounds from packaging polymers during microwave, conventional heat treatment, and storage. *Compr. Rev. Food Sci. Food Saf.* **12**, 523–545 (2013).
34. N. Dulal, R. Shanks, T. Gengenbach, H. Gill, D. Chalmers, B. Adhikari, I. P. Martinez, Slip-additive migration, surface morphology, and performance on injection moulded high-density polyethylene closures. *J. Colloid Interface Sci.* **505**, 537–545 (2017).
35. E. R. Jerison, Y. Xu, L. A. Wilen, E. R. Dufresne, Deformation of an elastic substrate by a three-phase contact line. *Phys. Rev. Lett.* **106**, 186103 (2011).
36. N. B. Vargaftik, B. N. Volkov, L. D. Voljak, International tables of the surface tension of water. *J. Phys. Chem. Ref. Data* **12**, 817–820 (1983).
37. A. S. Nielsen, D. N. Batchelder, R. Pyrz, Estimation of crystallinity of isotactic polypropylene using Raman spectroscopy. *Polymer* **43**, 2671–2676 (2002).
38. A. Gopanna, R. N. Mandapati, S. P. Thomas, K. Rajan, M. Chavali, Fourier transform infrared spectroscopy (FTIR), Raman spectroscopy and wide-angle x-ray scattering (WAXS) of polypropylene (PP)/cyclic olefin copolymer (COC) blends for qualitative and quantitative analysis. *Polym. Bull.* **76**, 4259–4274 (2019).
39. EU, Commission Regulation (EU) 2020/1245 of 2 September 2020 amending and correcting Regulation (EU) No 10/2011 on plastic materials and articles intended to come into contact with food. 2020.
40. S. I. Tamim, J. B. Bostwick, Plateau-Rayleigh instability in a soft viscoelastic material. *Soft Matter* **17**, 4170–4179 (2021).
41. D. Li, E. D. Sheerin, Y. Shi, L. Xiao, L. Yang, J. J. Boland, J. J. Wang, Alcohol pretreatment to eliminate the interference of micro additive particles in the identification of microplastics using Raman spectroscopy. *Environ. Sci. Technol.* **56**, 12158–12168 (2022).
42. T. Wang, S. Zhao, L. Zhu, J. C. McWilliams, L. Galgani, R. M. Amin, R. Nakajima, W. Jiang, M. Chen, Accumulation, transformation and transport of microplastics in estuarine fronts. *Nat. Rev. Earth Env.* **3**, 795–805 (2022).
43. E. Hernandez, B. Nowack, D. M. Mitrano, Polyester textiles as a source of microplastics from households: A mechanistic study to understand microfiber release during washing. *Environ. Sci. Technol.* **51**, 7036–7046 (2017).
44. L. W. Wang, M. S. Bank, J. Rinklebe, D. Hou, Plastic-rock complexes as hotspots for microplastic generation. *Environ. Sci. Technol.* **57**, 7009–7017 (2023).
45. W. L. Ryan, E. A. Hemmingsen, Bubble formation in water at smooth hydrophobic surfaces. *J. Colloid Interface Sci.* **157**, 312–317 (1993).
46. Z. Lei, C. Dai, B. Chen, Gas solubility in ionic liquids. *Chem. Rev.* **114**, 1289–1326 (2014).
47. R. Marks, Dissolved oxygen supersaturation and its impact on bubble formation in the southern Baltic Sea coastal waters. *Hydrol. Res.* **39**, 229–236 (2008).
48. P. S. Epstein, M. S. Plesset, On the stability of gas bubbles in liquid-gas solutions. *J. Chem. Phys.* **18**, 1505–1509 (1950).

49. D. Li, P. Li, Y. Shi, E. D. Sheerin, Z. Zhang, L. Yang, L. Xiao, C. Hill, C. Gordon, M. Ruether, J. Pepper, J. E. Sader, M. A. Morris, J. J. Wang, J. J. Boland, Stress-induced phase separation in plastics drives the release of amorphous polymer micropollutants into water. *Nat. Commun.* **16**, 3814 (2025).
50. E. R. Zettler, T. J. Mincer, L. A. Amaral-Zettler, Life in the "plastisphere": Microbial communities on plastic marine debris. *Environ. Sci. Technol.* **47**, 7137–7146 (2013).
51. Y. Wang, X. Chen, F. Wang, N. Cheng, Influence of typical clay minerals on aggregation and settling of pristine and aged polyethylene microplastics. *Environ. Pollut.* **316**, 120649 (2023).
52. Y. Shi, D. Li, L. Xiao, D. Mullarkey, D. K. Kehoe, E. D. Sheerin, S. Barwich, L. Yang, Y. K. Gun'ko, I. V. Shvets, M. E. Möbius, J. J. Boland, J. J. Wang, Real-world natural passivation phenomena can limit microplastic generation in water. *Chem. Eng. J.* **428**, 132466 (2022).
53. V. Onink, M. L. A. Kaandorp, E. van Sebille, C. Laufkötter, Influence of particle size and fragmentation on large-scale microplastic transport in the Mediterranean Sea. *Environ. Sci. Technol.* **56**, 15528–15540 (2022).
54. M. L. A. Kaandorp, D. Lobelle, C. Kehl, H. A. Dijkstra, E. van Sebille, Global mass of buoyant marine plastics dominated by large long-lived debris. *Nat. Geosci.* **16**, 689–694 (2023).
55. A. F. R. M. Ramsperger, V. K. B. Narayana, W. Gross, J. Mohanraj, M. Thelakkat, A. Greiner, H. Schmalz, H. Kress, C. Laforsch, Environmental exposure enhances the internalization of microplastic particles into cells. *Sci. Adv.* **6**, eabd1211 (2020).
56. N. S. Dhillon, J. Buongiorno, K. K. Varanasi, Critical heat flux maxima during boiling crisis on textured surfaces. *Nat. Commun.* **6**, 8247 (2015).
57. R. Evans, Z. Deng, A. K. Rogerson, A. S. McLachlan, J. J. Richards, M. Nilsson, G. A. Morris, Quantitative interpretation of diffusion-ordered NMR spectra: Can we rationalize small molecule diffusion coefficients. *Angew. Chem. Int. Ed.* **52**, 3199–3202 (2013).
58. A. Karami, A. Golieskardi, C. K. Choo, V. Larat, T. S. Galloway, B. Salamatinia, The presence of microplastics in commercial salts from different countries. *Sci. Rep.* **7**, 46173 (2017).
59. B. E. Oßmann, G. Sarau, S. W. Schmitt, H. Holtmannspötter, S. H. Christiansen, W. Dicke, Development of an optimal filter substrate for the identification of small microplastic particles in food by micro-Raman spectroscopy. *Anal. Bioanal. Chem.* **409**, 4099–4109 (2017).
60. D. Schymanski, C. Goldbeck, H.-U. Humpf, P. Fürst, Analysis of microplastics in water by micro-Raman spectroscopy: Release of plastic particles from different packaging into mineral water. *Water Res.* **129**, 154–162 (2018).
61. M. Lindner, Effect of substrate strain, aluminum thickness and corona pretreatment on the electrical resistance of physical vapor deposited aluminum coatings. *Coatings* **10**, 1245 (2020).

Acknowledgments: We appreciate the professional help from technician teams of Trinity Civil, Structural, and Environmental Department, Photonics Laboratory and AML in CRANN/AMBER Research Center. **Funding:** This work was supported by Science Foundation Ireland grants 20/FIP/PL/8733, 12/RC/2278_P2, and 16/IA/4462 (J.J.B. and J.J.W.), Research Ireland grant 24/PATH-S/12599 (D.L. and J.J.B.), Enterprise Ireland grant CF-2021-1729-1 (L.X. and D.L.), Enterprise Ireland grant CF-20180870 (J.J.W. and L.X.), the National Natural Science Foundation of China (52570216), and Advanced Talents Project by Zhejiang A&F University RC2024F01 (D.L.). **Author contributions:** J.J.B. led the overall effort. Conceptualization and supervision: J.J.B., L.X., J.J.W., and D.L. Methodology and data collection: Y.S., V.B., S.J., R.U., E.D.S., P.K., C.H., M.R., L.Z., X.P., Q.Z., H.Q., M.C., and J.E.S. Water sample collection and detection: Q.Y. and B.Z. Writing—original draft: D.L. and J.J.B. Writing—review and editing: J.J.B. and L.X. All authors discussed the results and commented on the manuscript. **Competing interests:** The authors declare that they have no competing interests. **Data and materials availability:** All data and code needed to evaluate and reproduce the results in the paper are present in the paper and/or the Supplementary Materials.

Submitted 10 July 2025
Accepted 20 November 2025
Published 17 December 2025
10.1126/sciadv.aea4729

ScienceAdvances

Microbubble-induced erosion releases micro- and nanoplastics into water

Dunzhu Li, Varvara Bolikava, Yunhong Shi, Songheng Jin, Richard Unitt, Emmet D. Sheerin, Peiying Kang, Liwen Xiao, Xiaocheng Pan, Christopher Hill, Manuel Ruether, Linfei Zhao, Qidong Yin, Bo Zhao, Qiliang Zhu, Hua Qin, Ming Cheng, John E. Sader, Jing Jing Wang, and John J. Boland

Sci. Adv. **11** (51), eaea4729. DOI: 10.1126/sciadv.aea4729

Science Advances (ISSN 2375-2548) is published by the American Association for the Advancement of Science. 1200 New York Avenue NW, Washington, DC 20005. The title *Science Advances* is a registered trademark of AAAS.